Materials Science & Engineering A 736 (2018) 344–348

Contents lists available at ScienceDirect

Materials Science & Engineering A

journal homepage: www.elsevier.com/locate/msea

Grain size dependence of strain rate sensitivity in a single phase *FCC* high entropy alloy $Al_{0.3}CoCrFeNi$

Sindhura Gangireddy[a,*], Bharat Gwalani[a,b], Rajiv S. Mishra[a,b]

[a] *Advanced Materials and Manufacturing Processes Institute, University of North Texas, Denton, TX 76207, United States*
[b] *Materials Science and Engineering, University of North Texas, Denton, TX 76207, United States*

ARTICLE INFO

Keywords:
Strain-rate sensitivity
Grain size dependence
Dynamic mechanical behavior
FCC high entropy alloy
$Al_{0.3}CoCrFeNi$

ABSTRACT

High-entropy alloys (HEAs) can offer exceptional strain-rate sensitivity (SRS) due to high lattice-friction and strong solid-solution strengthening, and in some cases, low stacking fault energy. In this study, SRS of a single phase FCC HEA- $Al_{0.3}CoCrFeNi$ was investigated at two grain sizes. Due to its outstanding Hall-Petch coefficient, grain size becomes a crucial microstructural feature in determination of strength and SRS. Change in SRS due to grain refinement was derived to be inversely proportional to associated strength gain, in coarse microstructures where grain size > > dislocation forest cell size. This correlation was proven using two microstructures with grain sizes of 12 μm and 150 μm, with yield strengths of 313 MPa and 145 MPa, and demonstrated SRS of m = 0.029 and 0.064, respectively. SRS was also derived to increase linearly with strength contribution from thermal short-range obstacles. The slope reflects the maximum upper limit on SRS possible upon elimination of all other obstacles of long-range nature. This limiting value of SRS was derived to be 0.118 for this HEA.

1. Introduction

High-entropy alloys (HEAs) are a new paradigm of metallic alloy development of stabilizing simple microstructures with multiple principal elements in equimolar proportions. Multi-element effects such as high entropy, sluggish diffusion, lattice distortion, and cocktail effects were proposed and extensively studied [1–4]. But HEAs can also offer outstanding strain-rate sensitivities (SRS). In typical *FCC* metals, internal strength is considered insignificant. But in HEAs, large friction stress values were reported due to significant lattice distortion and varying dislocation mobility [5]. They are reported to have large Peierls-Nabarro barriers as Wu et al. [6] observed from severe temperature dependence of tensile properties of CoCrFeMnNi HEA. With multitude of solute atoms, HEAs also show strong solid solution strengthening [7]. Moreover a low stacking fault energy (SFE), such as expected in $Al_xCoCrFeNi$ HEA system [8], causes dislocations to split into wide partials [9], and their cross-slip needs more thermal activation resulting in further contribution to an enhanced SRS. In this study, we investigated the grain size dependence of SRS in *FCC* HEAs via $Al_{0.3}CoCrFeNi$, which has low SFE, is precipitation hardenable at high temperatures, and shows remarkable Hall-Petch strengthening [9]. The alloy was studied in single phase form using two recrystallized microstructures of fine (12 μm) and coarse (150 μm) grain sizes. Alteration of microstructure by grain refinement was discovered to cause momentous variation in SRS.

2. Experimental procedure

The thermomechanical processing treatment steps for attaining the two grain sizes are summarized in Fig. 1. The cast alloy was first homogenized at high temperature for eliminating elemental segregation (1150 °C/10 min), then cold rolled to 60% thickness reduction, and subsequently solutionized once again at high temperature of 1150 °C for complete recrystallization. The hold duration (2–60 min) was varied to control the extent of grain growth. In all the heating steps, the samples were placed in the furnace after set temperature was reached and cooled by water quenching after specified treatment time. These microstructures were studied using scanning and transmission electron microscopes (SEM, TEM) and electron back-scatter diffraction (EBSD). Samples were subjected three mechanical testing procedures: a computer-controlled mini-tensile testing machine at an initial strain-rate of 10^{-3} s^{-1}, a pneumatic engine driven compression at a strain-rate of 10^{1} s^{-1}, in addition to dynamic deformation using a Split-Hopksinson Pressure Bar at a strain rate of 2×10^{3} s^{-1}.

3. Results and discussion

The thermomechanical processing treatments, 60% cold work

* Corresponding author.
E-mail address: sindhura.gangireddy@unt.edu (S. Gangireddy).

https://doi.org/10.1016/j.msea.2018.09.009
Received 22 June 2018; Received in revised form 28 August 2018; Accepted 4 September 2018
Available online 05 September 2018
0921-5093/

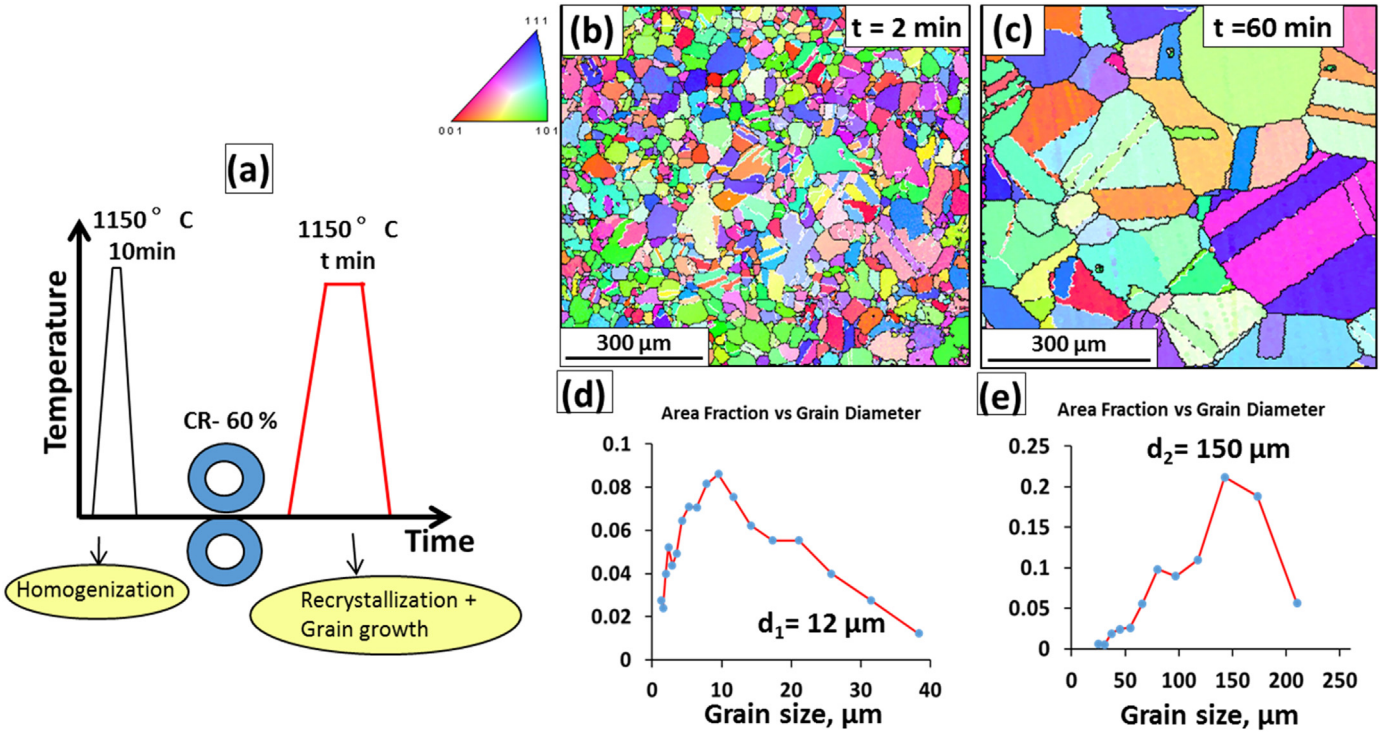

Fig. 1. (a) Thermomechanical processing steps, (b-c) EBSD images of the two recrystallized microstructures formed after solutionizing at high temperature for 2 min and 60 min hold time, (d-e) respective resultant recrystallized grain sizes: 12 µm from 2 min hold, 150 µm from grain growth during longer hold of 60 min.

followed by high temperature solutionization, yielded fully recrystallized microstructures. After a brief hold time of 2 min, a fine grained microstructure of 12 µm grain size was observed. Further holding to longer durations, 60 min, resulted in considerable grain growth and a coarser microstructure of 150 µm size was formed. EBSD images of these two microstructures and their grain size distributions are depicted in Fig. 1.

TEM and XRD examination of the microstructure formed within 2 min of hold time conclusively determined recrystallization of single phase FCC. Fig. 2(a) shows a bright field TEM image of a recrystallized FCC grain whose selected area diffraction patterns (SADP) from both [001] and [011] *FCC* zone axes showed only the fundamental *FCC* reflections, see Figs. 2(b) and 2(c). The XRD pattern of this microstructure, in Fig. 2(d), also showed only FCC diffraction peaks, (111) (200) (220), confirming recrystallization of FCC single phase.

The true stress-strain curves from mechanical testing at the three different strain-rate regimes are displayed in Fig. 3. With grain refinement, both quasi-static, interemediate, and dynamic flow stresses increased. The quasi-static yield strength had increased from σ_2= 14 MPa in the coarse 60 min homogenized condition with d_2= 15 µm to σ_1= 31 MPa in the f 2 min homogenized material with d_1= 1 2 µm.

The total flow stress can be given by a summation of internal stresses, dislocation hardening, and grain boundary strengthening:

$$\sigma = \sigma_o + \alpha\sqrt{\rho} + \frac{\beta}{\sqrt{d}} \quad (1)$$

where the first term accounts for both lattice friction and solid solution strength contributions, the second term for Taylor contribution, and the third arising from Hall-Petch relationship. Unlike conventional *FCC* alloys, the internal stress contributions would not be trivial in HEAs due

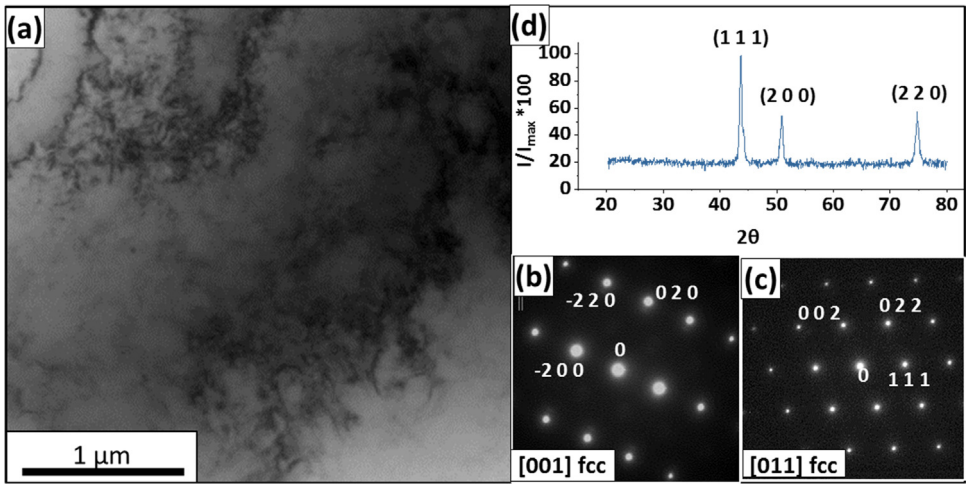

Fig. 2. (a) Bright Field TEM image showing a recrystallized grain with (b-c) SADP patterns from [001] and [011] zone axes, respectively, both showing only fundamental FCC reflections, (d) XRD showing FCC peaks (111), (200), (220) confirming single phase structure.

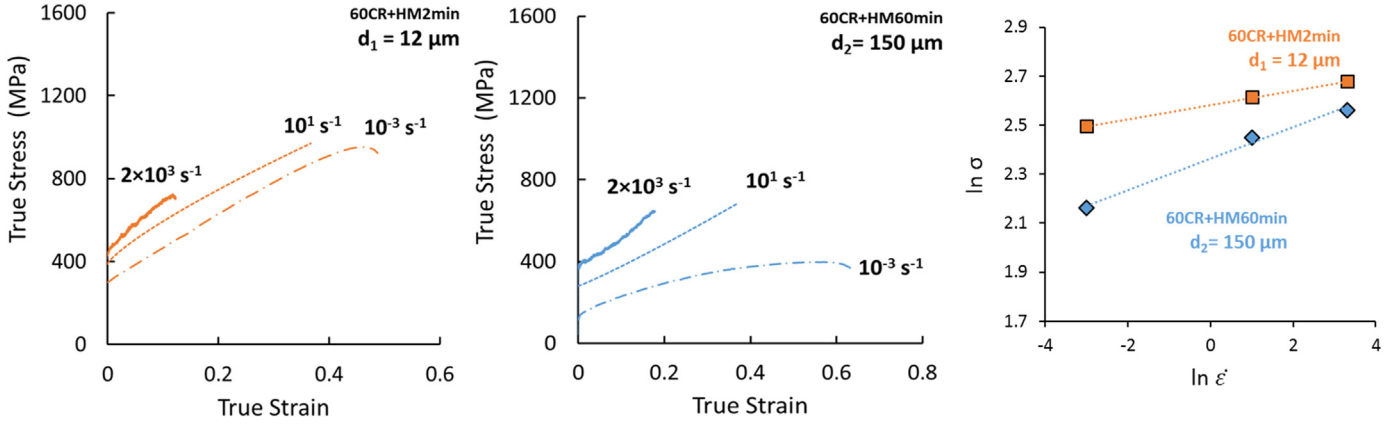

Fig. 3. Mechanical response of from quasi-static (10^{-3} s^{-1}) and dynamic (2×10^{3} s^{-1}) strain-rate regime testing: (a) 12 μm grainsize from 2 min homogenization, (b) 150 μm from 60 min homogenization. (c) Difference in the strain rate dependence of the two grain sizes demonstrated through logarithm of flow stress vs logarithm of strain rate (lnσ–lnε) graph.

to high lattice friction [5,6] and significant solid solution strengthening [7]. As both these recrystallized structures are in a relaxed state, they are expected to have low dislocation densities of the order of $\rho_0 = 10^{12}$ m^{-2}, typical in annealed metals [10] and dislocation hardening can be considered insignificant. So the difference in quasi-static yield strength is attributed to grain boundary strengthening and the Hall-Petch constant, β, can be derived as:

$$\beta = \frac{\sigma_1 - \sigma_2}{\frac{1}{\sqrt{d_1}} - \frac{1}{\sqrt{d_2}}} = 811\text{MPa}/\mu\text{m}^{0.5} \tag{2}$$

This value is quite close to that of 824 MPa/$\mu m^{0.5}$ reported by Gwalani et al. [11].

Compared to the ominous increase in quasi-static yield stress from 145 MPa to 313 MPa (an enhancement of 115%), the dynamic flow stress improved only from 365 MPa to 476 MPa, a mere 30%. This indicated that the strain-rate sensitivity (SRS), a measure of amplification of strength at higher strain-rates, varied significantly with grain size. The strain-rate sensitivity parameter, m,

$$m = \left[\frac{\partial ln\sigma}{\partial ln\dot{\varepsilon}}\right]_{T,\ \varepsilon} \tag{3}$$

can be calculated from the slope of logarithm of flow stress vs logarithm of strain rate ($ln\sigma - ln\dot{\varepsilon}$) graph, as demonstrated in Fig. 3(c). Estimates of strain-rate sensitivity parameter, m, of the two recrystallized conditions are summarized in Table 1.

SRS of the coarse grained 60 min homogenized material was exceptionally high at m = 0.064. Typically such large values were only reported in nano-crystalline *FCC* metals [12,13]. But HEAs appear to have extraordinary properties in strain-rate dependence as well. Li et al. [14] also have reported high SRS of 0.053 in another coarse grained microstructure of single phase *FCC* $Al_{0.3}$CoCrFeNi. With grain refinement, SRS was observed to drop sharply to nearly half, m = 0.029. This

Table 1
Summary of quasi-static strength, dynamic flow stress, and strain-rate sensitivities of the two microstructures with different grain sizes.

	Quasi-static strength $\dot{\varepsilon}$= 10^{-3} s^{-1}	Intermediate strength $\dot{\varepsilon}$= 10^{1} s^{-1}	Dynamic strength $\dot{\varepsilon}$= 10^{3} s^{-1}	m
60CR + HM2min (d_1 = 12 μm)	313	411	476	0.029
60CR + HM60min (d_2 = 150 μm)	145	281	365	0.064

behavior can be understood from the physical origin of flow stress activation volume (v^*) based on its definition as the rate of decrease of activation enthalpy with respect to flow stress. Taylor et al. [15] have derived:

$$v^* = -\frac{\partial \Delta H(\sigma)}{\partial \tau} = k_B T\left(\frac{\partial ln\dot{\gamma}}{\partial \tau}\right) \tag{4}$$

From the constitutive relationship between flow stress and strain-rate, $\sigma = K\dot{\varepsilon}^m$ or $\tau = K\dot{\gamma}^m$,

$$\frac{\partial ln\dot{\gamma}}{\partial \tau} = \frac{\frac{\partial ln\dot{\gamma}}{\partial \dot{\gamma}}}{\frac{\partial \tau}{\partial \dot{\gamma}}} = \frac{\frac{1}{\dot{\gamma}}}{K\dot{\gamma}^{m-1}} = \frac{1}{K\dot{\gamma}^m} = \frac{1}{\tau}$$

$$v^* = k_B T\frac{\tau}{m}$$

$$m = \frac{\sqrt{3}k_B T}{\sigma v^*} \tag{5}$$

The Becker's activation volume can also be defined in terms of dislocation motion [16]:

$$v^* = b \times \omega \times l \tag{6}$$

where b is the Burgers vector of the dislocations, ω is the distance swept out by the mobile dislocation during one activation event, and l is the Friedel sampling length representing average contact distance between two obstacles.

$$m = \frac{\sqrt{3}k_B T}{\sigma \times b \times \omega \times l} = \frac{\sqrt{3}k_B T}{b\omega} \cdot \frac{1}{\sigma \times l} \tag{7}$$

The first factor will be invariant for a given material, but the second factor would depend on the microstructural condition. An analysis of the terms, σ and l, can shed light on the rate controlling mechanisms. The flow stress, σ, is given in Eq. (1). The obstacle spacing, l, is roughly the average forest spacing for large-grained *FCC* metals with forest cutting as the dominant mechanism. Even as $Al_{0.3}$CoCrFeNi HEA was reported to twin extensively [14], slip is always the preceding mechanism as per Mahajan hypothesis [17]. For these SRS calculations based on yield stress, dislocation motion would be the dominant mechanism of plastic deformation. As forest spacing scales with dislocation density, l can be given by $\frac{c}{\sqrt{\rho}}$ with c as a proportionality constant. So SRS can be written as:

Table 2
Summary of thermal stress, yield stress, dynamic flow stress, relative contribution of internal stresses to total yield stress, and strain-rate sensitivity of the different microstructural conditions.

	$\sigma_0(\dot{\varepsilon} = 10^{-3})$ (MPa)	σ_{GB} (MPa)	$\sigma(\dot{\varepsilon} = 10^{-3})$ (MPa)	$\sigma(\dot{\varepsilon} = 2 \times 10^{3})$ (MPa)	$\frac{\sigma_0(\dot{\varepsilon} = 10^{-3})}{\sigma(\dot{\varepsilon} = 10^{-3})}$	$m=\left[\frac{\partial ln\sigma}{\partial ln\dot{\varepsilon}}\right]$
60CR + HM60min (d_1 = 12 μm)	78	235	313	476	0.249	0.029
60CR + HM2min (d_2 = 150 μm)	78	67	145	365	0.538	0.064
Limit case					0	0

$$m = \frac{\sqrt{3}k_BT}{b\omega}.\frac{1}{\left(\sigma_o + \alpha\sqrt{\rho} + \frac{\beta}{\sqrt{d}}\right)\frac{c}{\sqrt{\rho}}} = \frac{\sqrt{3}k_BT}{b\omega}.\frac{1}{\left(\frac{\sigma_o c}{\sqrt{\rho}} + \alpha c + \frac{\beta c}{\sqrt{\rho}\sqrt{d}}\right)} \tag{8}$$

Therefore as grain size, d, decreases, the denominator on RHS would decrease, and SRS would increase. With exceptionally large Hall-Petch constant of β = 811 MPa/μm$^{0.5}$ (derived in Eq. (2)), the effect would be more pronounced in this HEA.

In both the recrystallized conditions, the grain size is much larger than the controlling length scale typically on the order of nm. So for both conditions, the obstacle spacing l, would be invariant at small strains. Likewise, ω is also considered a constant [13]. Both the stress-strain curves were acquired at room temperature and at small strains, so adiabatic heating at dynamic strain-rates would also be minimal.

$$\frac{m_1}{m_2} = \frac{\frac{\sqrt{3}k_BT}{b\omega}.\frac{1}{\sigma_1 \times l}}{\frac{\sqrt{3}k_BT}{b\omega}.\frac{1}{\sigma_2 \times l}} = \frac{\sigma_2}{\sigma_1} \tag{9}$$

$$m_1 = \frac{\sigma_2}{\sigma_1}.\, m_2 \tag{10}$$

We can therefore estimate that the change in SRS due to grain size refinement would be inversely proportional to the associated strength gain. As Hall-Petch coefficient was very strong in this material, grain size reduction from 150 μm to 12 μm yielded strength gains of over 115%. Hence, SRS reduced drastically. From Eq. (10), SRS of the 12 μm fine grained structure can be estimated to be 0.029. This matched perfectly with the experimentally observed m = 0.029. The SRS reported by Li et al. in a coarse grained microstructure of single phase *FCC* $Al_{0.3}$CoCrFeNi [14] had slightly finer size than our 60 min homogenized structure and hence a lower SRS, m = 0.053.

The initial dislocation density in these recrystallized structures, which are in a relaxed state, can be expected to be very low [10]. So we can consider Taylor contribution in Eq. (1) to be insignificant.

$$\sigma = \sigma_o + \frac{\beta}{\sqrt{d}} \tag{11}$$

The first term, σ_o, is composed of internal stresses from short-range obstacles which are thermally activated, whereas the second term from grain boundary strengthening, $\sigma_{GB} = \frac{\beta}{\sqrt{d}}$ is long-range in nature and is an athermal contributor.

Eq. (3) of calculation of engineering strain-rate sensitivity, m, from two stress-strain curves acquired at different strain-rates is derived from visco-plastic constitutive function:

$$\sigma = K\dot{\varepsilon}^m \tag{12}$$

where K is a constant and σ is the total flow stress, as given by Eq. (11). In a limiting scenario, where grain size d- > ∞, σ_{GB}- > 0. If SRS of such a microstructural condition is m_0:

$$\sigma_0(\dot{\varepsilon}) = K\dot{\varepsilon}^{m_0} \tag{13}$$

Eq. (13) therefore captures the strain-rate sensitivity of the thermal stresses alone. Hence m_0 represents a limiting value for the maximum SRS that can be attained. Taking derivative of Eq. (12) with respect to strain-rate, $\dot{\varepsilon}$:

$$\begin{aligned} \frac{d\sigma}{d\dot{\varepsilon}} &= \frac{d\sigma_0(\dot{\varepsilon})}{d\dot{\varepsilon}} + \frac{d\sigma_{GB}}{d\dot{\varepsilon}} \\ Km\dot{\varepsilon}^{m-1} &= Km_0\dot{\varepsilon}^{m_0-1} + 0 \\ m\dot{\varepsilon}^{m-1} &= m_0\dot{\varepsilon}^{m_0-1} \\ \frac{\dot{\varepsilon}^{m_0}}{\dot{\varepsilon}^m} &= \frac{m}{m_0} \end{aligned} \tag{14}$$

As athermal stresses do not have strain = rate dependence, $\frac{d\sigma_{GB}}{d\dot{\varepsilon}} = 0$. So the relative contribution from thermal stresses to total strength can be written as:

$$\frac{\sigma_0}{\sigma} = \frac{K\dot{\varepsilon}^{m_0}}{K\dot{\varepsilon}^m} = \frac{\dot{\varepsilon}^{m_0}}{\dot{\varepsilon}^m}$$

From Eq. (14),

$$\frac{\sigma_0}{\sigma} = \frac{m}{m_0} \tag{15}$$

So SRS would increase linearly with relative contribution of thermal stress. From Hall-Petch constant calculated in Eq. (2), β = 811 MPa/μm$^{0.5}$, we can obtain internal stress from yield stress of 2 min homogenized condition as:

$$\sigma_o = \sigma_1 - \frac{\beta}{\sqrt{d_1}} = 78 \text{ MPa}. \tag{16}$$

The ratio of this thermal stress to total yield stress in the two conditions is compared to the experimentally observed SRS values in Table 2. A limiting case where thermal contributions approach zero, σ_o- > 0, resulting in the SRS also approaching zero m- > 0, is also included.

Fig. 4(a) compares thermal and athermal contributions in the two grain size conditions. Greater contribution from grain boundary strengthening in the finer grain size lead to a lowered SRS. Fig. 4(b) plots m as a function of $\frac{\sigma_0(\dot{\varepsilon})}{\sigma(\dot{\varepsilon})}$, and showed a linear relationship as expected from Eq. (15). The slope of this graph is m_0,the maximum SRS possible in this material, is 0.118.

4. Conclusions

Single phase *FCC*-based HEA $Al_{0.3}$CoCrFeNi is shown to be capable of demonstrating outstanding strain-rate sensitivity (SRS) at very coarse grain sizes. It has a remarkably high Hall-Petch strength coefficient, 811 MPa/μm$^{0.5}$, due to which grain refinement leads to significant strengthening. Yield strength increased from 145 MPa in 150 μm grain size to 313 MPa at 12 μm grain size. At these coarse grain sizes > > dislocation forest cell sizes, SRS is derived to be inversely proportional to strength. So grain refinement leads to sharp drop in SRS from m = 0.064 at 150 μm to m = 0.029 at 12 μm. SRS was also derived to linearly increase with thermal stress contributions, i.e. strength addition from short-range obstacles. When athermal contributions become negligible, such as in an extremely coarse or single grained microstructure, it is estimated that the SRS would approach a limiting value of 0.118.

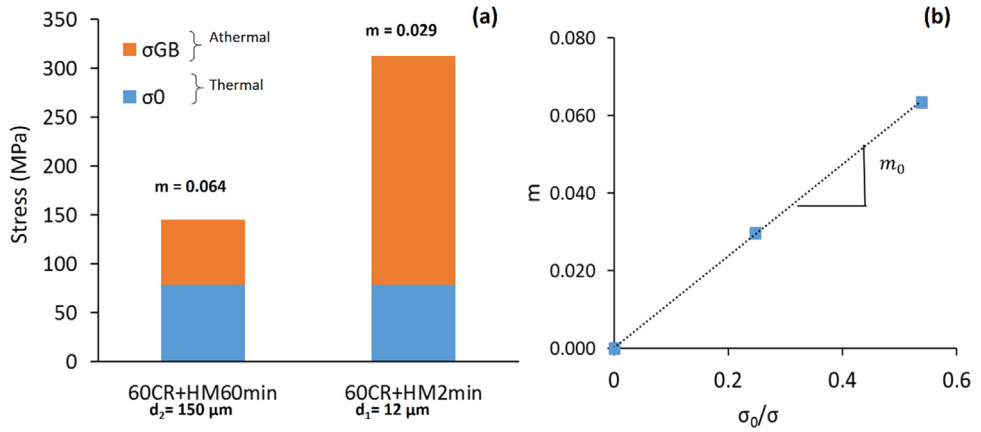

Fig. 4. (a) Plot showing the relative contributions from thermal internal stresses and athermal grain boundary strengthening to the total strength in the two recrystallized conditions with different grain sizes, and (b) variation of strain-rate sensitivity, m, with the fraction of thermal contribution to total yield stress, $\frac{\sigma_0}{\sigma}$, showing a linear relationship with slope $= m_0$, the limiting SRS.

Acknowledgment

The work was performed under cooperative agreement between Army Research Laboratory and University of North Texas (W911NF-16-2-0189). We also acknowledge Materials Research Facility at the University of North Texas for microscopy facilities.

Data availability

The raw data and the processing required to reproduce these findings are available to download and will be uploaded along with the manuscript.

References

[1] Y. Jien-Wei, Recent progress in high entropy alloys, Ann. Chim. Sci. Mater. 31 (6) (2006) 633–648.
[2] J.W. Yeh, Novel alloy concept, challenges and opportunities of high-entropy alloys, in: B. Raj (Ed.), Frontiers Design Materials, CRC Press, 2007, pp. 31–47.
[3] S. Ranganathan, Alloyed pleasures: multimetallic cocktails, Curr. Sci. 85 (5) (2003) 1404–1406.
[4] Y. Zhang, Y. Zhang, Y.J. Zhou, J.P. Lin, G.L. Chen, P.K. Liaw, Solid-solution phase formation rules for multi-component alloys, Adv. Eng. Mater. 10 (6) (2008) 534–538.
[5] N. Kumar, M. Komarasamy, P. Nelaturu, Z. Tang, P.K. Liaw, R.S. Mishra, Friction stir processing of a high entropy alloy $Al_{0.1}$CoCrFeNi, JOM 67 (5) (2015) 1007–1013.
[6] Z. Wu, Z. Wu, H. Bei, G.M. Pharr, E.P. George, Temperature dependence of the mechanical properties of equiatomic solid solution alloys with face-centered cubic crystal structures, Acta Mater. 81 (2014) 428–441.
[7] Y. Zhang, X. Yang, P.K. Liaw, Alloy design and properties optimization of high-entropy alloys, JOM 64 (7) (2012) 830–838.
[8] N. Kumar, Q. ing, X. Nie, R.S. Mishra, Z. Tang, P.K. Liaw, R.E. Brennan, K.J. Doherty, K.C. Cho, High strain-rate compressive deformation behavior of the $Al_{0.1}$CrFeCoNi high entropy alloy, Mater. Des. 86 (2015) 598–602.
[9] F. Otto, A. Dlouhý, C. Somsen, H. Bei, G. Eggeler, E.P. George, The influences of temperature and microstructure on the tensile properties of a CoCrFeMnNi high-entropy alloy, Acta Mater. 61 (15) (2013) 5743–5755.
[10] G.K. Williamson, R.E. Smallman, "Dislocation densities in some annealed and cold-worked metals from measurements on the X-ray Debye-Scherrer spectrum, Philos. Mag. 1 (1) (1956) 34–46.
[11] B. Gwalani, V. Soni, M. Lee, S.A. Mantri, Y. Ren, R. Banerjee, Optimizing the coupled effects of Hall-Petch and precipitation strengthening in a $Al_{0.3}$CoCrFeNi high entropy alloy, Mater. Des. 121 (2017) 254–260.
[12] R.Z. Valiev, I.V. Alexandrov, Y.T. Zhu, T.C. Lowe, Paradox of strength and ductility in metals processed by severe plastic deformation, J. Mater. Res. 17 (1) (2002) 5–8.
[13] Q. Wei, S. Cheng, K.T. Ramesh, E. Ma, Effect of nanocrystalline and ultrafine grain sizes on the strain rate sensitivity and activation volume: FCC versus bcc metals, Mater. Sci. Eng. A 381 (1–2) (2004) 71–79.
[14] Z. Li, S. Zhao, H. Diao, P.K. Liaw, M.A. Meyers, High-velocity deformation of Al0.3CoCrFeNi high-entropy alloy: remarkable resistance to shear failure, Sci. Rep. 7 (2017) 42742.
[15] G. Taylor, Thermally-activated deformation of BCC metals and alloys, Prog. Mater. Sci. 36 (1992) 29–61.
[16] J.W. Cahn, F.R.N. Nabarro, Thermal activation under shear, Philos. Mag. A 81 (5) (2001) 1409–1426.
[17] S. Mahajan, Critique of mechanisms of formation of deformation, annealing and growth twins: face-centered cubic metals and alloys, Scr. Mater. 68 (2) (2013) 95–99.